Increasing the efficiency of lanthanide luminescent bioprobes: bioconjugated silica nanoparticles as markers for cancerous cells†

Svetlana V. Eliseeva,[a] Bo Song,[a] Caroline D. B. Vandevyver,[a] Anne-Sophie Chauvin,[a] Josias B. Wacker[b] and Jean-Claude G. Bünzli*[ac]

Received (in Victoria, Australia) 8th June 2010, Accepted 11th August 2010
DOI: 10.1039/c0nj00440e

The lanthanide binuclear helicate $[Ln_2(L^{C2})_3]$ has been embedded into bare and NH_2-functionalized silica nanoparticles (NPs) using water-in-oil microemulsion technique. TEM analysis reveals both $[Ln_2(L^{C2})_3]@SiO_2$ and $[Ln_2(L^{C2})_3]@SiO_2/NH_2$ nanoparticles having a spherical morphology and being monodispersed with an average size of 55 ± 5 and 90 ± 10 nm, respectively. The energy of the ligand triplet state, ~21 800 cm^{-1} ($[Gd_2(L^{C2})_3]$@NP), does not change upon incorporation into silica nanoparticles and is optimal for sensitizing Eu^{III} luminescence. As a consequence, $[Eu_2(L^{C2})_3]@SiO_2$ and $[Eu_2(L^{C2})_3]@SiO_2/NH_2$ NPs display red emission due to characteristic $^5D_0 \rightarrow {}^7F_J$ (J = 0–4) transitions with absolute quantum yield reaching 28% for the latter. NH_2-functionalized NPs have then been conjugated with avidin (**NP-avidin**) or goat anti-mouse IgG antibody (**NP-IgG**) to test them as luminescent biomarkers. Time-resolved microscopy of immunocytochemical assays involving recognition of mucin-like proteins expressed on breast cancer MCF-7 cells by the 5D10 monoclonal antibody confirms that the **NP-IgG** bioprobe displays specific luminescent signal with signal-to-noise ratio ≈20% higher than the one obtained for the bioconjugate of molecular $[Eu_2(L^{C2(COOH)})_3]$ with IgG. In addition, immunoassays using a streptavidin-coated plate and the **NP-IgG** probe are able to detect 15 ng mL^{-1} of the biotinylated 5D10 antibody with a signal-to-noise ratio of 100.

Introduction

Since the advent of lanthanide-based time-resolved immunoassays in the late 1970's,[1] lanthanide luminescence has evolved into a ubiquitous and unavoidable tool in sensitive analytical bioassays and bioimaging.[2–5] The advantages of inserting the analytical probe into nanoparticles has been recognized in the early stages of the development of lanthanide luminescent probes.[6] Such nanobioprobes are now commonly used in multiple immunoassays under the form of up-converting phosphors[7,8] or in multicolor Vis-NIR tags.[9] Their general applications in biosciences have been recently reviewed.[10,11]

During the past five years, our laboratory has been developing a concept of binuclear lanthanide luminescent bioprobes (LLBs) which self-assemble in water at room temperature and physiological pH and which are thermodynamically stable and kinetically inert.[12] Their obvious advantage is the incorporation of two luminescent ions into one substrate, allied with potential heterometallic dual probe capability and chirality. The chelating platform with benzimidazolepyridine core is versatile enough to lend itself to various derivatizations, in particular in order to increase the hydrophilicity of the probe and to allow bioconjugation. The simple binuclear chelates $[Ln_2(L^{C2})_3]$ (Scheme 1) are highly luminescent (Ln = Eu, Tb) and can be considered to be non-cytotoxic (LD_{50} > 500 μM) for a range of cancerous and non-cancerous cells. They penetrate into these cells by endocytosis and localize into the endoplasmic reticulum, allowing time-resolved microscopy of live cells.[13] Upon derivatization with a carboxylic acid group, the resulting $[Ln_2(L^{C2(COOH)})_3]$ helicates are amenable to conjugation to avidin or various monoclonal antibodies providing sensitive and highly selective probes for the biomarkers expressed by cancerous cells and tissues.[14]

So far, the cells onto which we focused our attention have been human breast cancer MCF-7 cells. One way of detecting

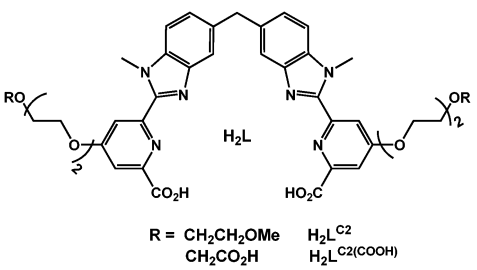

Scheme 1 Ditopic hexadentate ligands for the assembly of binuclear lanthanide helicates.

[a] *Ecole Polytechnique Fédérale de Lausanne (EPFL), Laboratory of Lanthanide Supramolecular Chemistry, BCH 1403, CH-1015 Lausanne, Switzerland. E-mail: jean-claude.bunzli@epfl.ch; Fax: +41 21 693 9825; Tel: +41 21 693 9821*
[b] *EPFL, Laboratory of Microsystems 2, BM 3130, CH-1015 Lausanne, Switzerland*
[c] *WCU Professor, Department of Advanced Materials Chemistry, Centre for Next Generation Photovoltaic Systems, Korea University, Sejong Campus, 208 Seochang, Jochiwon-eup, Yeongi-gun, ChungNam-do 339-700, South Korea*

† Electronic supplementary information (ESI) available: Description of synthesis of nanoparticle bioconjugates with avidin, comparison between luminescence spectra of un-doped SiO_2/NH_2 and doped with $[Eu_2(L^{C2})_3]$ nanoparticles (Fig. S1), and immunoluminescent detection of 5D10 Ag on MCF-7 cells by 5D10 with the **NP-IgG** probe (Fig. S2). See DOI: 10.1039/c0nj00440e

them is to target the mucin-like antigens expressed on the cell membrane by their corresponding 5D10 monoclonal antibody.[15,16] In turn, this antibody is recognized by an immunoglobulin decorated with the lanthanide chelate and which acts as species-specific secondary antibody. In this paper, we explore if improvement in sensitivity can be achieved with this successful model by replacing the molecular probe $[Eu_2(L^{C2(COOH)})_3]$ with silica nanoparticles doped with the simpler chelate $[Eu_2(L^{C2})_3]$ (Scheme 1). Full characterization of the nanoparticles as well as their photophysical properties are also reported.

Experimental

All chemicals were purchased from Aldrich or Fluka A.G. and used without further purification. $[Ln_2(L^{C2})_3]$ (Ln = Eu, Gd) were synthesized according to a previously described procedure.[17]

Synthesis

Nanoparticles doped with $[Ln_2(L^{C2})_3]$ (Ln = Eu, Gd)

Silica nanoparticles. 1.8 mL of *n*-hexanol were mixed with 7.5 mL of cyclohexane, followed by addition of 1.8 mL of Triton X-100, 400 μL of water, 80 μL of $[Ln_2(L^{C2})_3]$ solution in Tris-HCl (pH 7.4), and finally 100 μL of tetraethyl orthosilicate (TEOS). All steps were performed at 7 min intervals. The resulting solution was stirred for 30 min and 60 μL of 25% ammonia were added to facilitate the hydrolysis of TEOS. The reaction was continued for 24 h at rt.

NH_2-functionalized silica nanoparticles. Method 1 ("two-step"): Silica nanoparticles were first prepared as described above. Then, 50 μL of TEOS were added followed 30 min later by 10 μL of (3-aminopropyl)triethoxysilane (APS). The solution was stirred for additional 24 h.

Method 2 ("one step"): 1.8 mL of *n*-hexanol were mixed with 7.5 mL of cyclohexane, followed by addition of 1.8 mL of Triton X-100, 400 μL of water, 80 μL of $[Ln_2(L^{C2})_3]$ solution in Tris-HCl (pH 7.4) and finally, 73 μL of TEOS and 23 μL of APS were simultaneously added. Resulting solution was stirred for 30 min and 60 μL of 25% ammonia were added. The reaction was continued for 48 h at rt.

The concentration of the $[Ln_2(L^{C2})_3]$ solution varied from 0 (for pure silica nanoparticles) to 1 and 10 mM. The largest concentration was used for the biological tests. All micro emulsions were broken by addition of 10 mL of acetone and the nanoparticles were separated by centrifugation (3500 rpm), washed several times with ethanol and water and dried in air. For further use NPs were dispersed in the desired solvent under sonication. The average yield of NPs for all syntheses was ~15 mg.

Bioconjugates with goat anti-mouse IgG antibody (NP-IgG). 2 mg of NH_2-functionalized NPs (obtained using a 10 mM solution of $[Eu_2(L^{C2})_3]$) were washed twice with 2 mL of PBS (phosphate buffered saline, 0.01 M, pH 7.4) and then suspended in 2 mL of 7% glutaraldehyde solution in PBS, the reaction was run during 1 h 30 min at rt under continuous mixing. After washings with PBS (2×), NPs were suspended in 1.5 mL of PBS and 0.5 mL of 1 mg mL^{-1} aqueous solution of goat anti-mouse IgG Ab (M8645, Sigma) was added. The resulting solution was mixed for 3 h at rt, NPs were washed with PBS (3×), suspended in quenching solution (30 mM glycine in PBS containing 0.5% bovine serum albumin, BSA) and reacted for 30 min. After additional washings with PBS (3×) NPs were suspended in PBS with 0.05% BSA and stored at 4 °C before use.

Bioconjugates with avidin (NP-avidin). Bioconjugates with avidin (**NP-avidin**) were prepared according to a similar procedure as described for the bioconjugates with goat anti-mouse IgG Ab (see ESI†).

Leakage experiments. The extensive washing with PBS after isolation of the NPs did not result in a luminescence loss, even several months after their preparation, pointing to negligible leakage of the helicate out of the NPs.

Methods

IR spectra were recorded in the range 4000–600 cm^{-1} with a Perkin-Elmer SpectrumOne spectrometer equipped with a universal attenuated total reflection sampler. Transmission electron microscopy (TEM) was performed at the Interdisciplinary Centre for Electron Microscopy (CIME-EPFL) using a Philips FEI CM20 microscope. Emission, excitation spectra and lifetimes were measured with a Fluorolog FL3-22 spectrofluorimeter from Horiba-Jobin-Yvon Ltd. using 2 mm id quartz capillaries. All spectra were corrected for the instrumental functions. Luminescence decays were analyzed with Origin® and proved to be single-exponential functions in all cases. Quantum yields were determined with the Fluorolog spectrofluorimeter at room temperature under excitation into ligand states and according to an absolute method[18] using a home-modified integration sphere.[19] A capillary containing MgO was used to determine the intensity of excitation light (L_a, eqn (3) in ref. 19). Each sample was measured several times under slightly different experimental conditions. The estimated accuracy is ±10%.

Biotin-binding ELISA

A streptavidin-coated 96-well plate (DELFIA® yellow plate, AAAND-0005, PerkinElmer) was washed three times with 200 μL of DELFIA wash solution (DELFIA® wash concentrate, PerkinElmer Wallac Oy, Turku, Finland) and 100 μL of the appropriate dilutions of the biotinylated 5D10 antibody (10, 5, 1, 0.5, 0.1, 0.05, 0.01, 0.005, 0.001, 0.0001 and 0.00001 μg mL^{-1}) in DELFIA assay buffer (DELFIA® assay buffer, PerkinElmer Wallac Oy, Turku, Finland) was added to the wells, followed by 1 h incubation at rt. Subsequently to three more washings with wash solution, 100 μL of detection probe (200 μg mL^{-1} for **NP-IgG** or 5 μg mL^{-1} for the bioconjugate of $[Eu_2(L^{C2(COOH)})_3]$ with IgG (**Eu-IgG**))[14] were deposited in each well and incubated for 1 h at rt. Finally, after washings with DELFIA wash solution (5 × 200 mL), the luminescence was detected with the Victor 3 multi-label counter from PerkinElmer (λ_{ex} = 340 nm, λ_{em} = 615 nm, 0.4 ms delay time, 0.4 ms counting time, 1 ms cycling time). The detection limit was calculated as DL = (3SD × c)/(I_c − I_0), where SD is the standard deviation, c the first concentration giving a

detectable signal, I_c the emission intensity observed at concentration c, and I_0 the background intensity. The signal/noise ratio was calculated as $(I_{max} - I_0)/I_0$, where I_{max} is the maximum luminescence intensity.

MCF-7 cell immunoluminescent assays

With bioconjugates with goat anti-mouse IgG antibody. MCF-7 cells were grown on an 8-well μ-slide (ibidi, Basel) for 12 h, and after washing the slide three times with PBS, the cells were fixed with 0.4% glutaraldehyde for 15 min at rt. They were subsequently washed four times with DELFIA wash solution and treated with 150 μL of DELFIA assay buffer for 30 min at rt. The primary antibody, 5D10 (10 μg mL^{-1}) was added in the wells, followed by 1 h incubation at rt. After further washings with wash solution (4 × 200 mL), the detection conjugates, **NP-IgG** (400 μg mL^{-1}) or **Eu-IgG** (10 μg mL^{-1}), were added to each well and incubated for an additional 1 h at rt. Finally, the slides were washed 4× with 200 mL wash solution and immunoluminescence was measured with a home-modified time-resolved luminescence setup Signifier from Wallac Oy equipped with a Nikon Eclipse 600 microscope and an ORCA-ER CCD camera (Hamamatsu): λ_{exc} = 340 nm (bandpass filter, BP = 70 nm); λ_{em} = 420 nm (longpass LP filter); excitation pulse length, 10 μs; delay time, 100 μs, gate time, 600 μs; exposure time, 30 s; 10× or 40× PlanFluo objectives.

With bioconjugates with avidin. The general procedure was similar except that biotinylated 5D10 (10 μg mL^{-1}) was used as primary antibody. In an effort to reduce the background signal various washing procedures (0.05% Tween 20 in PBS, or 0.05% Triton X-100 in PBS, or DELFIA wash buffer, or 0.05% Tween 20 in sodium carbonate solution, pH 9.0) and blocking (1% BSA in PBS, or 1% Casein in Tris-HCl, pH 7.4, or 5% FCS in PBS, or antibody diluent from DAKO) buffers were tested.

Results and discussion

Synthesis and characterization of NPs doped with $[Ln_2(L^{C2})_3]$ (Ln = Eu, Gd)

Bare nanoparticles were prepared in a water-in-oil micro emulsion consisting of an aqueous solution of $[Ln_2(L^{C2})_3]$ (Ln = Gd, Eu) helicate, Triton X-100 surfactant, *n*-hexanol co-surfactant, and cyclohexane as oil phase, by controlling the hydrolysis of TEOS with aqueous ammonia.[20] For synthesizing amino-derivatized NPs, the same micro emulsion was used but two different ways of adding silane reagents were tested: (1) a "two-step method", in which APS was added after hydrolysis of TEOS for ≈24 h, and (2) a "one-step method", where TEOS and APS were added simultaneously in an optimal ratio $V_{TEOS}/V_{TEOS+APS}$ = 0.73.[21] The functional groups on the surface of the NPs were identified by IR spectroscopy (Fig. 1). For NPs doped with $[Ru(bpy)_3]^{2+}$, it was reported that the first procedure results in the formation of NPs displaying more intense luminescence and having more surfacial NH_2 groups in comparison with the "one-step method". The explanation for the lower concentration of the dye inside NPs was found in

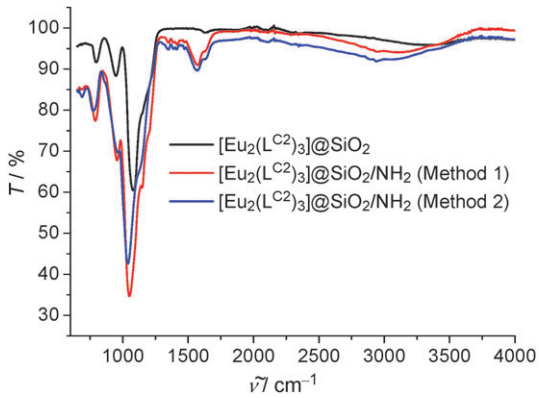

Fig. 1 IR spectra of Eu-containing silica NPs.

repelling of positive $[Ru(bpy)_3]^{2+}$ molecules by protonated amine groups from APS in the "one-step" procedure. However, in our case the complex is neutral and a contrary result was were obtained: the "two-step" method led to the isolation of poorly luminescent NPs while when TEOS and APS were added simultaneously the obtained Eu^{III} NPs displayed bright luminescence with photophysical parameters more comparable to those of $[Eu_2(L^{C2})_3]@SiO_2$ nanoparticles (see below).

Surface modification of the nanoparticles with NH_2 groups results in appearance of additional bands of $\delta(NH_2)$ and ν(N–H) vibrations in the ranges 1570–1610 and 2800–3400 cm^{-1}, respectively, compared to bare NPs. IR spectra of all NPs also display strong bands corresponding to valence Si–O (950–1200 cm^{-1}) and Si–C (760–790 cm^{-1}) vibrations.

TEM analysis revealed both $[Eu_2(L^{C2})_3]@SiO_2$ and $[Eu_2(L^{C2})_3]@SiO_2/NH_2$ nanoparticles having a spherical morphology and being monodispersed with an average size of 55 ± 5 and 90 ± 10 nm, respectively (Fig. 2).

If we consider that all helicate molecules are included into the nanoparticles, and taking into account the average diameter (d) of the NPs as well as the yield from synthesis (η), we can estimate the average number of helicates entrapped into one NP:

$$N_1 = \frac{N_m}{N_{NP}} = \frac{cVN_A}{\eta/m_{NP}} = \frac{cVN_A\left(\frac{1}{6}\pi\rho_{NP}d^3\right)}{\eta} \qquad (1)$$

in which N_m is the number of complex molecules in the initial solution, N_{NP} the average number of NPs obtained from synthesis, c the concentration and V the volume of the helicate

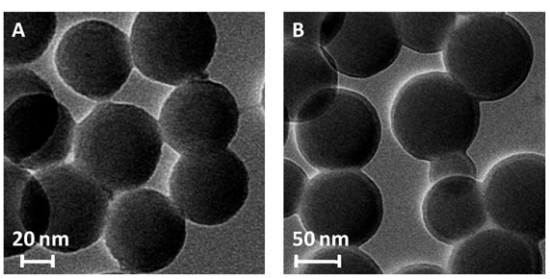

Fig. 2 TEM images of (A) $[Eu_2(L^{C2})_3]@SiO_2$ and (B) $[Eu_2(L^{C2})_3]@SiO_2/NH_2$.

solution; N_A is Avogadro's number, m_{NP} the mass and ρ_{NP} the density (taken equal to the one of pure silica, 1.95 g cm^{-3}) of NPs. Thus we find for a 1 mM helicate starting solution that ≈540 (pure silica) and ≈2380 (NH_2-derivatized NPs) complex molecules are inserted into one nanoparticle.

Photoluminescent properties

Ligand-centered luminescence. To establish if the incorporation of lanthanide helicates into silica nanoparticles affects the properties of the organic ligand, in particular the energy of the triplet state, $[Gd_2(L^{C2})_3]@SiO_2$ and $[Gd_2(L^{C2})_3]@SiO_2/NH_2$ were synthesized. The two phosphorescence spectra of the solid state NPs present a broad band with maximum at ~490 nm and featuring an extended vibrational progression. In addition, the spectrum of the amino-derivatized NPs exhibits a shoulder at ~410 nm which does not disappear after enforcing a 0.1 ms delay (Fig. 3). The energies of the ligand triplet states, estimated from the 0-phonon transitions, are the same and amount to ~21 800 cm^{-1}. This value is comparable with the one reported for a solution of $[Gd_2(L^{C2})_3]$, ~21 900 cm^{-1},[17] thus confirming that incorporation of $[Gd_2(L^{C2})_3]$ into silica nanoparticles does not influence the triplet state energy of the organic ligand. Luminescence decays (λ_{ex} = 307 nm, λ_{em} = 490 nm) are monoexponential and correspond to lifetimes of 7.1(2) and 6.8(2) ms for $[Gd_2(L^{C2})_3]@SiO_2$ and $[Gd_2(L^{C2})_3]@SiO_2/NH_2$, respectively. These values are about 20% shorter than the lifetime reported for a solution of $[Gd_2(L^{C2})_3]$, 8.7 ms.[17]

Metal-centered luminescence. Excitation spectra of solid state samples of $[Eu_2(L^{C2})_3]$-embedded nanoparticles are similar to those of the initial Eu^{III} helicate (Fig. 4) and present broad bands in the range 250–370 nm due to the ligand electronic transitions; no sharp bands corresponding to Eu^{III} f–f transitions are seen. Under excitation into ligand levels (330 nm) all NPs display the narrow and characteristic red luminescence due to $^5D_0 \rightarrow {}^7F_J$ (J = 0–4) transitions (Fig. 4). In addition to the metal-centered emission, NH_2-functionalized NPs exhibit a weak blue luminescence centered at ~400 nm and arising from the silica shell (Fig. S1, ESI†). The ligand-field splitting patterns identified from the luminescence spectra only show slight differences between the two kinds of NPs and are quite comparable to those of the parent $[Eu_2(L^{C2})_3]$ complex. On the other hand, incorporation of the helicate into NPs results in an increase in the relative integral intensities of the $^5D_0 \rightarrow {}^7F_2$ and $^5D_0 \rightarrow {}^7F_4$ transitions and therefore in higher values of I_{tot}/I_{MD} by ≈20–40% (Table 1).

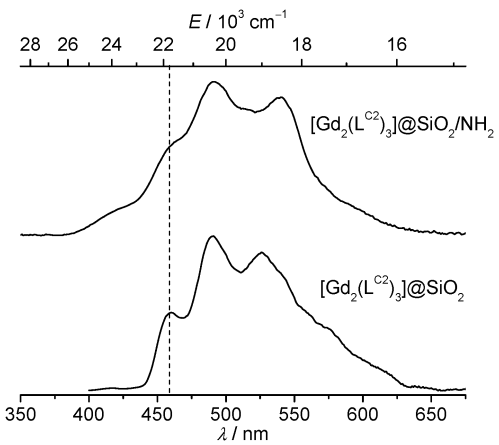

Fig. 3 Phosphorescence spectra of solid state $[Gd_2(L^{C2})_3]@SiO_2$ and $[Gd_2(L^{C2})_3]@SiO_2/NH_2$ nanoparticles (λ_{ex} = 307 nm, 0.05 ms delay, T = 77 K).

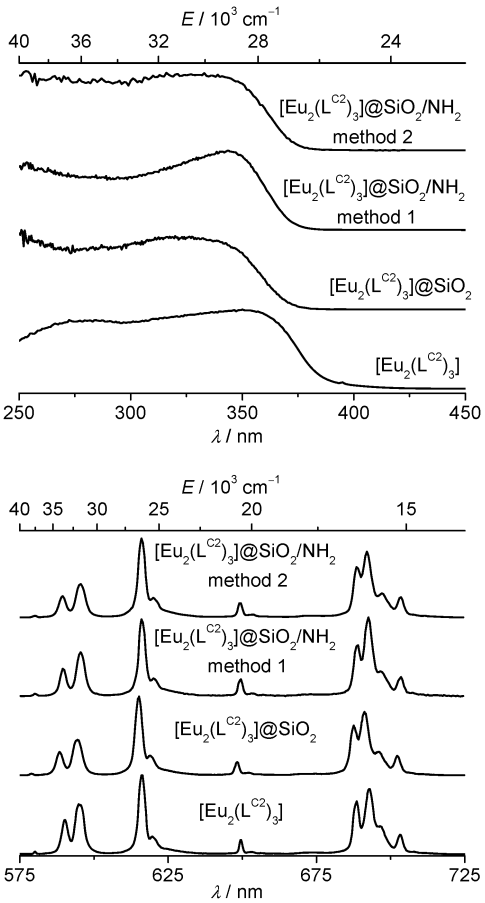

Fig. 4 (Top) Excitation and (bottom) emission spectra (λ_{ex} = 330 nm) of solid state samples of pure $[Eu_2(L^{C2})_3]$ and of $[Eu_2(L^{C2})_3]$-imbedded silica NPs at room temperature.

The luminescence lifetimes (τ_{obs}) of the $^5D_0$ level for $[Eu_2(L^{C2})_3]@SiO_2$ and NH_2-functionalized NPs obtained by the "one-step method" are long, 2.50(3) and 2.40(2) ms, respectively, and comparable with the one for solid state $[Eu_2(L^{C2})_3]$ (Table 2). The slight decrease in going from pure silica to amine-derivatized silica is consistent with the larger size of the latter NPs.[22] That is, incorporation of the helicate into the nanoparticles does not decrease non-radiative de-activations since the wrapping of the three ligand strands around the two metal ions provides highly protective coordination environments. As mentioned above, $[Eu_2(L^{C2})_3]@SiO_2/NH_2$ NPs synthesized by the "two-step method" are less luminescent and τ_{obs} is consequently shorter, concomitant with a significant decrease in the ligand-excited luminescence quantum yield Q^L_{Eu} to 6%. The quantum yield for the other $[Eu_2(L^{C2})_3]@SiO_2/NH_2$ NPs, obtained by method 2, is slightly larger compared to the one of the parent helicate, while pure silica NPs have the same

Table 1 Relative integrated intensities of the $^5D_0 \rightarrow {}^7F_J$ (J = 0–4) transitions for solid state samples of $[Eu_2(L^{C2})_3]$ and the corresponding doped silica NPs at 295 K (λ_{ex} = 330 nm)

Compound	$\int_{0-0}$	$\int_{0-1}$	$\int_{0-2}$	$\int_{0-3}$	$\int_{0-4}$	I_{tot}/I_{MD}
$[Eu_2(L^{C2})_3]$	0.01	1.00	1.10	0.09	1.94	4.14
$[Eu_2(L^{C2})_3]@SiO_2$	0.01	1.00	1.61	0.16	2.60	5.38
$[Eu_2(L^{C2})_3]@SiO_2/NH_2$ (method 1)	0.01	1.00	1.36	0.17	2.52	5.06
$[Eu_2(L^{C2})_3]@SiO_2/NH_2$ (method 2)	0.01	1.00	1.79	0.19	2.91	5.90

Table 2 Photophysical parameters for solid state samples of $[Eu_2(L^{C2})_3]$ and the corresponding silica NPs (λ_{ex} = 330 nm)[a]

Compound	τ_{obs}/ms	Q^L_{Eu} (%)	τ_{rad}[b]/ms	Q^{Eu}_{Eu}[b] (%)	η_{sens}[b] (%)
$[Eu_2(L^{C2})_3]$[c]	2.36(1)	24(1)	4.9	48	50
$[Eu_2(L^{C2})_3]@SiO_2$	2.50(3)	23(1)	4.2	60	38
$[Eu_2(L^{C2})_3]@SiO_2/NH_2$ (method 1)	1.85(2)	6(1)	4.4	42	14
$[Eu_2(L^{C2})_3]@SiO_2/NH_2$ (method 2)	2.40(2)	28(1)	3.8	63	44

[a] Data for 295 K unless otherwise stated. Standard deviation (2σ) between parentheses; estimated relative errors: τ_{obs}, ±2%; Q^L_{Ln}, ±10%; τ_{rad}, ±10%; Q^{Eu}_{Eu}, ±12%; η_{sens}, ±22%. [b] See eqn (2) and eqn (3) for definitions, n is taken equal to 1.5 for $[Eu_2(L^{C2})_3]$ or to 1.45 for silica NPs. [c] From ref. 23.

quantum yield as the parent helicate, within experimental reproducibility.

Intrinsic quantum yields (Q^{Eu}_{Eu}) could not be measured because of the low intensity of f–f transitions and have therefore been estimated from the calculated radiative lifetime as described in the following equations:[24,25]

$$Q^{Eu}_{Eu} = \frac{\tau_{obs}}{\tau_{rad}} \quad (2a)$$

$$\frac{1}{\tau_{rad}} = A_{MD,0} n^3 \left(\frac{I_{tot}}{I_{MD}}\right) \quad (2b)$$

with $A_{MD,0}$ being a constant equal to 14.65 s^{-1} and (I_{tot}/I_{MD}) the ratio of the total integrated $^5D_0 \rightarrow {}^7F_J$ emission (taken as J = 0–4) to the integrated intensity of the $^5D_0 \rightarrow {}^7F_1$ transition. The refractive index n could not be measured experimentally, but it has been set equal to 1.5 for $[Eu_2(L^{C2})_3]$, a value commonly encountered in complexes with organic ligands,[19,26] or to 1.45 for silica NPs. Of course, a small variation in n can generate a large error on τ_{rad}, so that absolute values have to be taken with great care since the refractive index of NPs is also size dependent.[22] Nevertheless, this estimate is useful to unravel general trends. Compared to the parent helicate, the radiative lifetime of the doped nanoparticles is 10–22% shorter. The smaller value occurs for $[Eu_2(L^{C2})_3]@SiO_2/NH_2$ (method 2), followed by $[Eu_2(L^{C2})_3]@SiO_2$. This drop is responsible for the enhanced Q^{Eu}_{Eu} values for these two samples (reaching ≈60%); the refractive index factor ($1.45^3/1.5^3$) contributes to increase the radiative lifetime by about 10% while the larger I_{tot}/I_{MD} ratio decreases it by ≈30–40% (Table 1). The sensitization efficiency of the ligand can now be calculated from:

$$\eta_{sens} = \left(\frac{Q^L_{Eu}}{Q^{Eu}_{Eu}}\right) \quad (3)$$

The corresponding data reported in Table 2 show a small decrease, at the limit of significance, for $[Eu_2(L^{C2})_3]@SiO_2$ and $[Eu_2(L^{C2})_3]@SiO_2/NH_2$ (method 2) NPs with respect to the parent helicate. On the other hand, it appears clearly that the large drop in overall quantum yield for the $[Eu_2(L^{C2})_3]@SiO_2/NH_2$ NPs synthesized by the 2-step method is almost entirely due to a largely reduced energy transfer, the ligand excited states being probably de-activated by a fast non-radiative process. Interestingly enough, when Q^L_{Eu} values are corrected for the absorption of silica, by using the corresponding $[Gd_2(L^{C2})_3]@SiO_2$ or $[Gd_2(L^{C2})_3]@SiO_2/NH_2$ (method 2) samples for the determination of L_a (see eqn (3), ref. 19), they almost match the Q^{Eu}_{Eu} values. This means that incorporation of the helicates into the SiO_2 NPs avoids non-radiative energy dissipation in the ligands and favors transfer to the Eu^{III} ion.

Bioconjugation of the NPs and corresponding bio-assays. One goal of our work is the specific targeting of cancerous cells. To this end, NH_2-functionalized nanoparticles were initially conjugated to avidin (see ESI†) in order to take advantage of the strong avidin–biotin interaction. However, time-resolved microscopy images evidenced a large background noise indicating important non-specific binding of the lanthanide luminescent probe on the surface of the MCF-7 cells. This background luminescence persisted despite thorough washing according to different protocols (see Experimental part). Therefore, the Eu-doped NH_2-functionalized NPs were directly conjugated to a goat anti-mouse IgG polyclonal antibody, a specific probe for the 5D10 monoclonal antibody and indirect immunoassays were performed. A standard coupling procedure was used in which the surfacial NH_2 groups were first activated with glutaraldehyde as a cross-linking agent and then reacted with a 3-fold excess of IgG with respect to a monolayer coating of the NPs surface (Scheme 2). The amount S of IgG needed to achieve surface saturation can be estimated by the following equation: $S = (6/\rho_S d)(C)$, where S is in units of mg of protein g^{-1} of NP, ρ_S is density of the NP (taken as 1.95 g cm^{-3} for silica), d the mean diameter (μm) and C the capacity of microsphere surface for a given protein, ~3 and 2.5 mg m^{-2} for BSA (MW = 65 kD), and bovine IgG (MW = 150 kD), respectively. For the sake of comparison

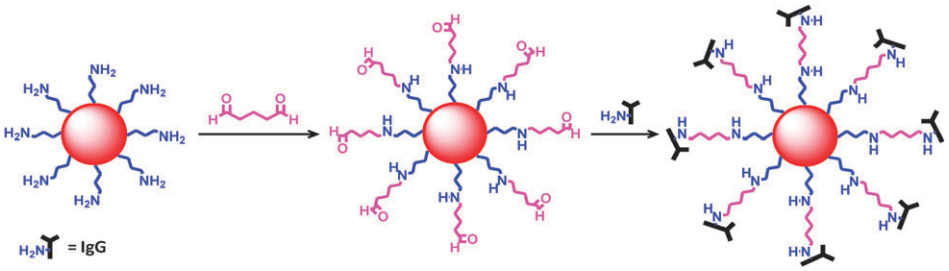

Scheme 2 Bioconjugation of NH_2-functionalized silica NPs with goat anti-mouse IgG antibody.

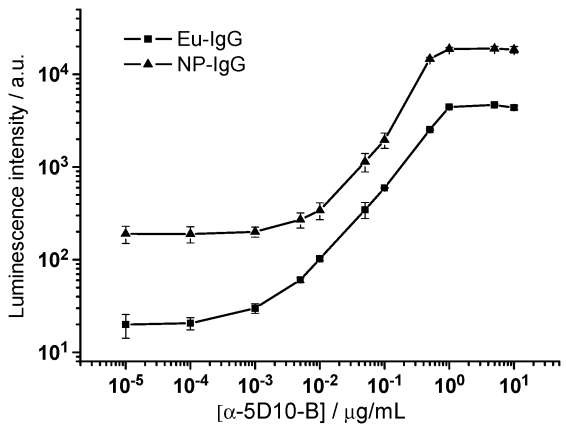

Fig. 5 Absolute emission intensity of **NP-IgG** and **Eu-IgG** as a function of the biotinylated 5D10 antibody concentration.

the bioconjugate of $[Eu_2(L^{C2(COOH)})_3]$ with the same antibody (**Eu-IgG**) was also prepared.[14]

Immunoassays were performed using a streptavidin-coated 96-well plate and increasing concentration of biotinylated 5D10 mAb as primary antibody. Time-resolved detection of luminescence intensity showed that the intensity of the signal generated by the conjugated NPs was substantially larger compared to **Eu-IgG** (Fig. 5). However, the signal/noise (S/N) ratio for **NP-IgG** is only 100, while it reaches 150 for **Eu-IgG**. Consequently, the lowest detectable concentration of α-5D10-B giving a detectable signal is 15 and 1.7 ng mL^{-1} for **NP-IgG** and **Eu-IgG**, respectively. The lower S/N ratio of the **NP-IgG** probe in comparison with **Eu-IgG** can be caused by higher nonspecific binding of the former mainly due to electrostatic interactions between the silica and plastic plate, resulting in an increase of the background signal.[27,28] Alternatively, this could also arise from steric hindrance in view of the large size of the nanoparticles which somehow could restrict access of the luminescent **NP-IgG** to the mouse monoclonal Ab 5D10-B.[29]

Despite this somewhat deceptive result, the **NP-IgG** bioprobe was tested on breast cancer MCF-7 cells, which express mucin-like proteins recognizable by the 5D10 monoclonal antibody. A blank assay was conducted without

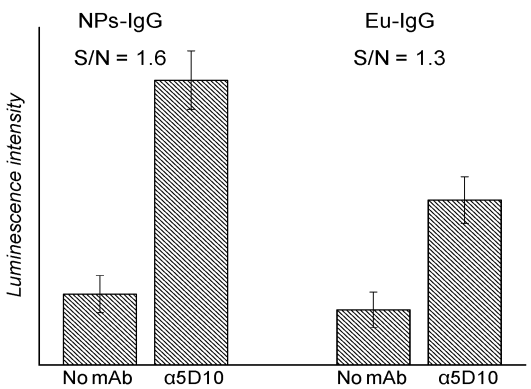

Fig. 7 Luminescence intensity of **NP-IgG** and **Eu-IgG** detection probes as a function of the presence of the 5D10 antigen on MCF-7 cells.

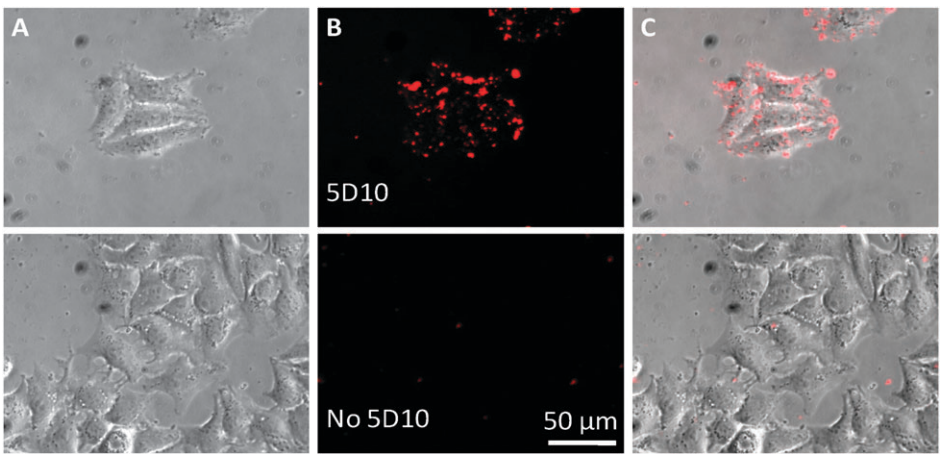

Fig. 6 Immunoluminescent detection of 5D10 Ag on MCF-7 cells by 5D10 with the **NP-IgG** probe: (A) bright field, (B) luminescence and (C) merged images.

5D10 antibody and the nanoparticle probe was again compared with **Eu-IgG**. The resulting time-resolved microscopy images of the immunoluminescent assay are shown in Fig. 6 (see also Fig. S2, ESI†) and confirm that the **NP-IgG** bioprobe displays specific immunoluminescent signal towards MCF-7 cells incubated with 5D10. The signal-to-noise ratio was estimated by integrating the luminescence intensity of 10 different areas of at least three different images of the microslide. In this case, contrary to ELISA experiment, the nanoparticle probe yields a 20% larger S/N ratio (1.6) than the molecular conjugate (1.3) (Fig. 7). Such a difference between the two experiments can be explained by the lower sensitivity of the CCD detector of the time-resolved microscope resulting in a less precise determination of the background signals.

Conclusions

We have demonstrated that the large $[Eu_2(L^{C2})_3]$ helicate (MW = 2823) can be easily embedded into pure silica monodispersed nanoparticles while retaining its photophysical properties. The isolation of amine-derivatized nanoparticles was less straightforward, being dependent on the synthetic path, but improved photophysical properties were obtained and these NPs could be conjugated to an IgG polyclonal antibody for target-specific bio-assays. The NP conjugate recognizes the 5D10 antibody expressed by cancerous MCF-7 cells and the signal-to-noise ratio obtained for the immunoluminescent assay is better than the one achieved with the molecular probe $[Eu_2(L^{C2(COOH)})_3]$ conjugated to the same antibody. The improvement ($\approx$20%) is less than expected but it is valuable in that it allows using a synthetically easier-to-obtain lanthanide chelate, namely $[Eu_2(L^{C2})_3]$[17] *versus* $[Eu_2(L^{C2(COOH)})_3]$.[14] This work further demonstrates the versatility of the helicate platform chosen for developing our bio-assay strategy since in addition to extensive derivatization[30] and multi-photon excitation[31] it can generate efficient and specific nanobioprobes.

Acknowledgements

This research is supported by the Swiss National Science Foundation (grant Nr. 200020_119866/1). We are grateful to Drs Virendra Kumar Parashar for discussions and Vanesa Fernandez-Moreira for providing the **Eu-IgG** bioconjugate. JCB thanks the WCU program from the National Science Foundation of Korea for grant R31-10035.

References

1 E. Soini and I. Hemmilä, *Clin. Chem. (Washington, DC)*, 1979, **25**, 353.
2 J.-C. G. Bünzli, *Chem. Rev.*, 2010, **110**, 2729.
3 S. V. Eliseeva and J.-C. G. Bünzli, *Chem. Soc. Rev.*, 2010, **39**, 189.
4 K. N. Allen and B. Imperiali, *Curr. Opin. Chem. Biol.*, 2010, **14**, 247.
5 C. P. Montgomery, B. S. Murray, E. J. New, R. Pal and D. Parker, *Acc. Chem. Res.*, 2009, **42**, 925.
6 D. S. Frank and M. W. Sundberg, *US Pat.*, 4,283,382, 1981.
7 D. E. Cooper, A. D'Andrea, G. W. Faris, B. MacQueen and W. H. Wright, in *Immunoassay and Other Bioanalytical Techniques*, ed. J. M. Van Emon, CRC Press Taylor & Francis group, Boca Raton, 2007, ch. 9, 217–247.
8 T. Soukka, T. Rantanen and K. Kuningas, *Ann. N. Y. Acad. Sci.*, 2008, **1130**, 188.
9 J. Samuel, G. Tallec, P. Cherns, W. L. Ling, O. Raccurt, O. Poncelet, D. Imbert and M. Mazzanti, *Chem. Commun.*, 2010, **46**, 2647.
10 F. Wang and X. Liu, *Chem. Soc. Rev.*, 2009, **38**, 976.
11 J. Shen, L. D. Sun and C. H. Yan, *Dalton Trans.*, 2008, 5687.
12 J.-C. G. Bünzli, A.-S. Chauvin, C. D. B. Vandevyver, B. Song and S. Comby, *Ann. N. Y. Acad. Sci.*, 2008, **1130**, 97.
13 B. Song, C. D. B. Vandevyver, A.-S. Chauvin and J.-C. G. Bünzli, *Org. Biomol. Chem.*, 2008, **6**, 4125.
14 V. Fernández-Moreira, B. Song, V. Sivagnanam, A.-S. Chauvin, C. D. B. Vandevyver, M. A. M. Gijs, I. A. Hemmilä, H.-A. Lehr and J.-C. G. Bünzli, *Analyst*, 2010, **135**, 42.
15 L. Plessers, E. Bosmans, A. Cox and J. Raus, *Anticancer Res.*, 1986, **6**, 885.
16 Y. Chin, L. Plessers, J. Vandepitte and J. Raus, *Eur. J. Cancer Clin. Oncol.*, 1991, **27**, 48.
17 A.-S. Chauvin, S. Comby, B. Song, C. D. B. Vandevyver and J.-C. G. Bünzli, *Chem.–Eur. J.*, 2008, **14**, 1726.
18 J. N. Demas and G. A. Crosby, *J. Phys. Chem.*, 1971, **75**, 991.
19 A. Aebischer, F. Gumy and J.-C. G. Bünzli, *Phys. Chem. Chem. Phys.*, 2009, **11**, 1346.
20 P. Sharma, S. Brown, M. Varshney and B. Moudgil, *Adv. Polym. Sci.*, 2008, **218**, 189.
21 S. Liu, H. L. Zhang, T. C. Liu, B. Liu, Y. C. Cao, Z. L. Huang, Y. D. Zhao and Q. M. Luo, *J. Biomed. Mater. Res., Part A*, 2007, **80a**, 752.
22 G. K. Liu and X. Y. Chen, in *Handbook on the Physics and Chemistry of Rare Earths*, ed. K. A. Gschneidner Jr, J.-C. G. Bünzli and V. K. Pecharsky, Elsevier Science B.V., Amsterdam, 2007, vol. 37, ch. 233.
23 J.-C. G. Bünzli, A.-S. Chauvin, H. K. Kim, E. Deiters and S. V. Eliseeva, *Coord. Chem. Rev.*, 2010, **254**(21–22), 2623.
24 J.-C. G. Bünzli and S. V. Eliseeva, in *Springer Series on Fluorescence. Lanthanide Luminescence: Photophysical, Analytical and Biological Aspects*, ed. P. Hänninen and H. Härmä, Springer Verlag, Berlin, 2010, vol. 8, ch. 3, published online July 15, DOI: 10.1007/4243_2010_3.
25 M. H. V. Werts, R. T. F. Jukes and J. W. Verhoeven, *Phys. Chem. Chem. Phys.*, 2002, **4**, 1542.
26 J. W. M. Verwey and G. Blasse, *Chem. Mater.*, 1990, **2**, 458.
27 T. Soukka, H. Härmä, J. Paukkunen and T. Lövgren, *Anal. Chem.*, 2001, **73**, 2254.
28 V. Sivagnanam, B. Song, C. Vandevyver and M. A. M. Gijs, *Anal. Chem.*, 2009, **81**, 6509.
29 H. Härmä, T. Soukka and T. Lövgren, *Clin. Chem.*, 2001, **47**, 561.
30 E. Deiters, B. Song, A.-S. Chauvin, C. Vandevyver and J.-C. G. Bünzli, *Chem.–Eur. J.*, 2009, **15**, 885.
31 S. V. Eliseeva, G. Auböck, F. van Mourik, A. Cannizo, B. Song, E. Deiters, A.-S. Chauvin, M. Chergui and J.-C. G. Bünzli, *J. Phys. Chem. B*, 2010, **114**, 2932.